INTERNATIONAL JOURNAL FOR NUMERICAL METHODS IN FLUIDS
Int. J. Numer. Meth. Fluids 2012; **69**:763–780
Published online 9 June 2011 in Wiley Online Library (wileyonlinelibrary.com/journal/nmf). DOI: 10.1002/fld.2607

Approximations of the Carrier–Greenspan periodic solution to the shallow water wave equations for flows on a sloping beach

Sudi Mungkasi[1,2,*,†] and Stephen G. Roberts[1]

[1]*Mathematical Sciences Institute, The Australian National University, Canberra, Australia*
[2]*Department of Mathematics, Sanata Dharma University, Yogyakarta, Indonesia*

SUMMARY

The Carrier–Greenspan solutions to the shallow water wave equations for flows on a sloping beach are of two types, periodic and transient. This paper focuses only on periodic-type waves. We review an exact solution over the whole domain presented by Johns ['Numerical integration of the shallow water equations over a sloping shelf', *Int. J. Numer. Meth. Fluids*, 2(3): 253–261, 1982] and its approximate solution (the Johns prescription) prescribed at the zero point of the spatial domain. A new simple formula for the shoreline velocity is presented. We also present new higher order approximations of the Carrier–Greenspan solution at the zero point of the spatial domain. Furthermore, we compare numerical solutions obtained using a finite volume method to simulate the periodic waves generated by the Johns prescription with those found using the same method to simulate the periodic waves generated by the Carrier–Greenspan exact prescription and with those found using the same method to simulate the periodic waves generated by the new approximations. We find that the Johns prescription may lead to a large error. In contrast, the new approximations presented in this paper produce a significantly smaller error. Copyright © 2011 John Wiley & Sons, Ltd.

Received 14 May 2010; Revised 14 April 2011; Accepted 15 April 2011

KEY WORDS: sloping beach; periodic waves; shallow water wave equations; finite volume methods; fixed boundary; moving shoreline

1. INTRODUCTION

The Carrier–Greenspan periodic solution [1] has been widely applied to test the performance of numerical methods used to solve the shallow water wave equations (consult [2–6] for example). This solution involves a fixed boundary and a moving boundary. To generate the periodic waves, either the Carrier–Greenspan exact solution or its approximation at the fixed boundary is prescribed.

Johns [5] presented a specific form of the Carrier–Greenspan exact solution of periodic type over a spatial domain and prescribed an approximate solution at the zero point of the spatial domain, where the fixed boundary is located. The approximate solution can be applied at the fixed boundary to generate an approximation of the Carrier–Greenspan exact solution using a numerical method as done by a number of authors, such as Johns [5] and Sidén and Lynch [6]. Thus, the numerical solution is affected by two sources of error, namely, the error in the boundary condition (at the fixed boundary) and the error introduced by the numerical discretization. Ideally, when testing a numerical method, we want to quantify the error introduced by the numerical discretization. However, testing a numerical method by prescribing the approximate solution at the fixed boundary may be misleading because the error in the boundary condition could be the dominant term. Note that the prescription at the fixed boundary propagates towards the moving boundary (shoreline), so the error at the fixed boundary also propagates towards the shoreline.

*Correspondence to: Sudi Mungkasi, Mathematical Sciences Institute, The Australian National University, Canberra, Australia.
†E-mail: sudi.mungkasi@anu.edu.au, sudi@usd.ac.id

Our main point is that, in general, the approximate solution of Johns [5] is unable to accurately estimate the Carrier–Greenspan exact solution at the zero point of the spatial domain. In addition, the large prescription error at the fixed boundary results in a large error of the solution generated by the numerical method. Therefore, we propose new approximations (which are more accurate than the approximate solution of Johns [5]) of the Carrier–Greenspan exact solution at the zero point of the spatial domain.

In this paper, we derive the formulation of Johns [5] for the Carrier–Greenspan periodic solution, as Johns [5] did not explicitly present the derivation. Based on that formulation, we then derive a new formula for the shoreline velocity and new approximate solutions at the zero point of the spatial domain. The new formula for the shoreline velocity is found using l'Hospital's Rule, and the new approximate solutions at the zero point of the spatial domain are found by extending the approximate solution of Johns [5] using either formal expansion or fixed point iteration.

The remainder of this paper is organized as follows. Section 2 recalls the shallow water wave equations in dimensional and dimensionless systems. Section 3 is devoted to the analytical work on the Carrier–Greenspan solution for periodic waves. In Section 4, two test cases are investigated, which verify our claim that the use of the Johns prescription can lead to large errors, and in addition, our new approximations are indeed more accurate. In Section 5, we present the rate of convergence of the numerical method used in the simulations. Finally, some concluding remarks are stated in Section 6.

2. GOVERNING EQUATIONS

The shallow water wave equations can be written in the standard dimensional system as well as the non-standard dimensionless system. These equations are the mathematical relations governing the vertically averaged hydrostatic water motion. In this section, we recall the shallow water wave equations in both systems. Equations in the dimensionless system are used for simplicity in the analytical work in Section 3, whereas equations in the dimensional system are utilized to easily understand the solution, physically, in the numerical experiments in Sections 4 and 5.

In the standard Cartesian coordinate system, the conservative shallow water wave equations consist of the mass and momentum equations

$$h^*_{t^*} + \left(h^* u^*\right)_{x^*} = 0, \tag{1}$$

$$\left(h^* u^*\right)_{t^*} + \left(h^* u^{*2} + \frac{1}{2} g h^{*2}\right)_{x^*} = -g h^* z^*_{x^*}. \tag{2}$$

Here, x^* represents the coordinate in one-dimensional space, t^* represents the time variable, $u^* = u^*(x^*, t^*)$ denotes the water velocity, $z^* = z^*(x^*)$ denotes the water bed topography, $h^* = h^*(x^*, t^*)$ denotes the water height, that is, the distance from the free surface to the water bed topography, and g is the constant of gravitation.

Consider the situation illustrated in Figure 1. The topography changes linearly with x^*

$$z^* = (h^*_0 / L^*) x^* - h^*_0, \tag{3}$$

in which h^*_0 is the vertical distance from the origin O to the topography at any time, and L^* is the horizontal distance from the origin O to the topography when the water is still. This implies that when the water is still, $z^* = -h^*$ over the spatial domain, $z^* = -h^*_0$ at $x^* = 0$, and the position of the shoreline is $x^* = L^*$.

We introduce a new variable called the stage $w^* := h^* + z^*$, which specifies the free surface. Scaling the horizontal distance by L^*, the vertical distance by h^*_0, the time by $L^*/\sqrt{g h^*_0}$, and the velocity by $\sqrt{g h^*_0}$, we can rewrite Equations (1) and (2) as the nonconservative dimensionless shallow water wave equations

$$w_t + [(w + 1 - x)\, u]_x = 0, \tag{4}$$

DOI: 10.1002/fld

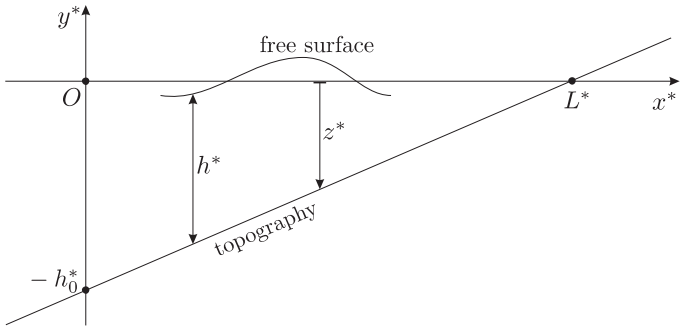

Figure 1. Cross section of a sloping beach.

$$u_t + uu_x + w_x = 0. \tag{5}$$

In this paper, all unstarred variables denote dimensionless quantities corresponding to their dimensional quantities denoted by starred variables. Equations (4) and (5) were used by Johns [5] in developing a finite difference numerical technique to simulate shallow water flows on a sloping beach.

Remark 1
For smooth solutions, Equations (4) and (5) are equivalent to the conservative dimensionless shallow water wave equations

$$h_t + (hu)_x = 0, \tag{6}$$

$$(hu)_t + \left(hu^2 + \frac{1}{2}h^2\right)_x = -hz_x. \tag{7}$$

3. PERIODIC WAVES ON A SLOPING BEACH

In this section, we review the solutions for periodic waves on a sloping beach presented by Carrier and Greenspan [1]. Five subsections are given. In Subsection 3.1, we recall the hodograph transformation applied by Carrier and Greenspan [1] to solve the shallow water equations analytically. This solution in the hodograph variables is then transformed back to the physical variables in Subsection 3.2 to get the formulation of Johns [5] for the Carrier–Greenspan periodic solution. We then present a new formula for the shoreline velocity in Subsection 3.3. In Subsection 3.4, we review the Johns approximation, which can be used as boundary conditions for numerical simulations, to the Carrier–Greenspan periodic solution at $x = 0$. Finally, Subsection 3.5 is devoted to new (more accurate) approximations of the Carrier–Greenspan periodic solution at $x = 0$.

3.1. Carrier–Greenspan solution

Carrier and Greenspan [1] applied the classical hodograph transformation to solve the shallow water wave equations. Two dimensionless hodograph variables

$$\sigma = 4c, \tag{8}$$

$$\lambda = 2(u + t) \tag{9}$$

were used. Here,

$$c = \sqrt{w + 1 - x} \tag{10}$$

is the wave speed relative to the water velocity u. In the hodograph system, the variables σ and λ are, respectively, a space-like and a time-like coordinate [3]. Note that the value of $w+1-x$ is

DOI: 10.1002/fld

actually the water height h in our dimensionless system. The dimensionless variables are related to the hodograph variables as

$$x = \frac{1}{4}\phi_\lambda - \frac{1}{16}\sigma^2 - \frac{1}{2}u^2 + 1, \quad t = \frac{1}{2}\lambda - u, \tag{11}$$

$$w = \frac{1}{4}\phi_\lambda - \frac{1}{2}u^2, \quad u = \sigma^{-1}\phi_\sigma, \tag{12}$$

where $\phi = \phi(\sigma, \lambda)$ is a potential function satisfying

$$(\sigma\phi_\sigma)_\sigma - \sigma\phi_{\lambda\lambda} = 0. \tag{13}$$

Equations for stage w and velocity u given by Equation (12) are the Carrier–Greenspan exact solution. The choice of $\phi(\sigma, \lambda)$, which satisfies Equation (13), depends on the conditions of the investigated problem.

Carrier and Greenspan [1] showed that a periodic oscillation of water is formed if we take

$$\phi(\sigma, \lambda) = AJ_0(\omega\sigma)\cos(\omega\lambda) \tag{14}$$

as long as the Jacobian $\partial(x, t)/\partial(\sigma, \lambda)$ does not vanish in $\sigma > 0$. This means that the implicit functions $w(x, t)$ and $u(x, t)$ are single-valued, that is, the waves represented by those functions do not break. Here, J_0 is the Bessel function of the first kind of order 0. The constant ω is given by π/T instead of the usual value $2\pi/T$ because a coefficient of 2 has appeared in the definition of λ in Equation (9), where T is the dimensionless period of oscillation. According to Equations (13) and (14), we can infer that

$$\phi(\sigma, \lambda) = AJ_0(\omega\sigma)\sin(\omega\lambda) \tag{15}$$

is also a potential function satisfying Equation (13).

3.2. The formulation of Johns for the Carrier–Greenspan periodic solution

In this subsection, we transform the solution (12) from the hodograph variables σ and λ to the usual variables x and t.

Considering the potential function (15), Johns [5] presented the corresponding Carrier–Greenspan periodic solution and prescribed an approximation of the Carrier–Greenspan periodic solution at $x = 0$. Here, we derive the formulation[‡] of Johns [5] for the Carrier–Greenspan periodic solution, so that in the next subsections we can propose a new formula for the shoreline velocity, review the prescription of Johns at $x = 0$, and propose new approximations of the Carrier–Greenspan periodic solution at $x = 0$. The motivation here is to provide the missing derivation of the solution presented by Johns [5].

Let us consider the potential function (15). Its partial derivatives are

$$\phi_\sigma = -\omega AJ_1(\omega\sigma)\sin(\omega\lambda), \tag{16}$$

$$\phi_\lambda = \omega AJ_0(\omega\sigma)\cos(\omega\lambda), \tag{17}$$

where J_1 and J_0 are Bessel functions of the first kind of order 1 and 0, respectively. Substituting Equations (16) and (17) into Equation (12), we obtain

$$w = -\frac{1}{2}u^2 + \frac{1}{4}\omega AJ_0(\omega\sigma)\cos(\omega\lambda), \tag{18}$$

[‡]Sidén and Lynch [6], in implementing the formulation of Johns, observed that the solution presented by Johns [5] fails to satisfy the kinematic boundary condition on the moving boundary because it involves a factor of 4. This failure is because of a misprint (typographical error) in the solution presented by Johns.

DOI: 10.1002/fld

$$u = -\frac{\omega A J_1(\omega\sigma)}{\sigma}\sin(\omega\lambda). \tag{19}$$

Letting $\mathcal{A} = \frac{1}{4}\omega A$ and recalling $\omega = \pi/T$, we can write Equations (18) and (19) as

$$w = -\frac{1}{2}u^2 + \mathcal{A}J_0\left(\frac{4\pi\alpha}{T}\right)\cos\left(\frac{2\pi\beta}{T}\right), \tag{20}$$

$$u = -\frac{\mathcal{A}J_1\left(\frac{4\pi\alpha}{T}\right)}{\alpha}\sin\left(\frac{2\pi\beta}{T}\right), \tag{21}$$

where $\alpha = c$ and $\beta = \frac{1}{2}\lambda$. Here, α and β have the same meaning as that used by Johns [5] but is different from that used by Carrier and Greenspan [1]. Equations (20) and (21) are the Carrier–Greenspan exact solution corresponding to the potential function (15).

For convenience, we rewrite the Carrier–Greenspan exact solutions (20) and (21) as

$$w = -\frac{1}{2}u^2 + \mathcal{A}J_0\left(\frac{4\pi\sqrt{w+1-x}}{T}\right)\cos\left(\frac{2\pi\,(u+t)}{T}\right), \tag{22}$$

$$u = -\frac{\mathcal{A}J_1\left(\frac{4\pi\sqrt{w+1-x}}{T}\right)}{\sqrt{w+1-x}}\sin\left(\frac{2\pi\,(u+t)}{T}\right). \tag{23}$$

3.3. Calculating the stage and velocity

Let us recall some properties of the shoreline before presenting how to calculate the stage w and velocity u over the whole domain. The shoreline is a moving boundary, and its position is defined at any time by $c = 0$, so that, introducing the dimensionless horizontal displacement ξ of the shoreline, by Equation (10), we have

$$\xi(t) = w(1 + \xi(t), t). \tag{24}$$

Differentiating Equation (24) with respect to t, we have

$$\frac{\mathrm{d}\xi}{\mathrm{d}t} = w_x\frac{\mathrm{d}\xi}{\mathrm{d}t} + w_t. \tag{25}$$

Using Equation (4) and assuming that $w_x(1+\xi(t), t) < 1$, we obtain the kinematical condition of the shoreline

$$u = \frac{\mathrm{d}\xi}{\mathrm{d}t} \quad \text{at} \quad x = 1 + \xi. \tag{26}$$

A statement of zero depth $c = 0$ at $x = 1+\xi$ and the kinematical condition (26) are the boundary conditions at the shoreline [5]. Note that because the slope of the topography in the dimensionless system is unity, we have $\xi = w$ at the shoreline, as described by Dietrich, Kolar, and Luettich [4]. This means that the horizontal displacement of the shoreline is equal to the vertical displacement of the shoreline. Because the instantaneous shoreline is fixed by the statement of zero depth $c = 0$ at $x = 1+\xi$, the horizontal displacement of the shoreline is

$$\xi = -\frac{1}{2}u^2 + \mathcal{A}\cos\left(\frac{2\pi(u+t)}{T}\right), \tag{27}$$

according to Equation (22).

DOI: 10.1002/fld

To test a numerical method, Dietrich *et al.* [4] used the Carrier–Greenspan solution by referring to the formulation[§] of Johns [5]. To figure out the solution, Dietrich *et al.* [4] took two steps. First, the system of equations consisting of the horizontal displacement ξ and the velocity u of the shoreline

$$\xi = -\frac{1}{2}u^2 + \mathcal{A}\cos\left(\frac{2\pi}{T}(u+t)\right), \tag{28}$$

$$u = \frac{\mathrm{d}\xi}{\mathrm{d}t} = -u\frac{\mathrm{d}u}{\mathrm{d}t} - \frac{2\mathcal{A}\pi}{T}\left(1+\frac{\mathrm{d}u}{\mathrm{d}t}\right)\sin\left(\frac{2\pi}{T}(u+t)\right) \tag{29}$$

were solved. Equation (29) was solved for velocity u using a finite difference approximation on the $\mathrm{d}u/\mathrm{d}t$ terms as well as using the information that the velocity of the shoreline at maximum inundation is zero. The shoreline displacement was found by substituting the shoreline velocity u into Equation (28). Second, the stage w and velocity u at the interior points in the wet region (on the left side of the shoreline) were calculated using Equations (22) and (23).

Here, we propose a different approach at the first step to find the shoreline velocity. Let us consider the velocity formulation (21) at wet areas, that is, on the interval $\alpha \geqslant 0$. We take the limit of the velocity formulation (21) as α goes to zero and take l'Hospital's Rule to get

$$u = -\frac{2\pi}{T}\mathcal{A}\sin\left(\frac{2\pi}{T}(u+t)\right), \tag{30}$$

which is our new formula for the shoreline velocity. Note that we take Equation (21), instead of Equation (23), into consideration in the derivation of Equation (30) because it is clearer to work with. Then the shoreline displacement is found by substituting the shoreline velocity u into Equation (28). The second step is similar to the work of Dietrich *et al.* [4]. To be specific, we can use the Newton–Raphson method to solve Equations (22) and (23) to get the stage w and velocity u of interior points in the wet region, with a note that the solution at a point closer to the shoreline is the initial guess for the Newton–Raphson method in obtaining the solution for a point further away from the shoreline.

3.4. The Johns approximate solution at the zero point of the spatial domain

In this subsection, we focus on the solution at spatial point $x = 0$ and review the prescription of Johns [5] defined at that point.

Let us assume that $w, u << 1$ at $x = 0$. At $x = 0$, Johns [5] prescribed the stage

$$w = \epsilon\cos\left(\frac{2\pi t}{T}\right), \tag{31}$$

where ϵ is the dimensionless wave amplitude, and fixed the amplitude factor $\mathcal{A}$ in terms of ϵ, which can be explained as follows. Let

$$w = w_0 + \delta w \quad , \quad u = u_0 + \delta u \tag{32}$$

be defined, where $w = w_0$, $u = u_0$ is a reference state, whereas δw and δu are perturbation terms. Substituting Equation (32) into the right-hand side of Equations (22) and (23) with a sea at rest $w_0 = 0$, $u_0 = 0$ as the reference state leads to

$$w = -\frac{1}{2}(\delta u)^2 + \mathcal{A}J_0\left(\frac{4\pi\sqrt{\delta w + 1}}{T}\right)\cos\left(\frac{2\pi(\delta u + t)}{T}\right), \tag{33}$$

[§]Dietrich *et al.* [4] used the analytical solution with a factor of 4 appearing in front of the amplitude factor in the formulation of the velocity $\boldsymbol{u}$. This suggests that the analytical solution that they used might not be the correct one. However, we cannot judge if they really used either the correct or incorrect formulation of the velocity $\boldsymbol{u}$ because there exists a variable $\boldsymbol{\alpha}$ involved in their formulation that is not described.

DOI: 10.1002/fld

$$u = -\frac{\mathcal{A}J_1\left(\frac{4\pi\sqrt{\delta w+1}}{T}\right)}{\sqrt{\delta w+1}}\sin\left(\frac{2\pi\,(\delta u+t)}{T}\right) \tag{34}$$

at $x=0$. Johns [5] took

$$w = \mathcal{A}J_0\left(\frac{4\pi}{T}\right)\cos\left(\frac{2\pi t}{T}\right), \tag{35}$$

$$u = -\mathcal{A}J_1\left(\frac{4\pi}{T}\right)\sin\left(\frac{2\pi t}{T}\right), \tag{36}$$

which are explicit functions of time t and linear with respect to the amplitude $\mathcal{A}$. This means that all contributions of perturbation terms δw and δu on the right-hand side of Equations (33) and (34) are neglected.

Matching Equation (35) with Equation (31), Johns [5] fixed

$$\mathcal{A} = \frac{\epsilon}{J_0\left(\frac{4\pi}{T}\right)}, \tag{37}$$

which is the amplitude factor $\mathcal{A}$ in terms of ϵ. We note that the assumption made on w and u in the linearization of Johns ($w, u << 1$ at $x=0$) implies $\mathcal{A} << 1$. However, the amplitude factor $\mathcal{A}$ given by Equation (37), which implies the quality of approximation (35) and (36), is determined by two elements. The first is, rather intuitively, the magnitude of ϵ, whereas the second is the denominator $J_0(4\pi/T)$. As a result, we can have significant nonlinear effects even for moderate values of ϵ, which will be demonstrated in Section 4.

In this paper, Equation (35) is called 'the Johns approximate solution' of the Carrier–Greenspan exact solution for the stage w at $x = 0$ or 'the Johns prescription' when it is applied at a fixed boundary to generate a periodic wave using a numerical method. Note that the value of the amplitude factor $\mathcal{A}$ corresponds to the maximum shoreline displacement (see the explanation of Carrier and Greenspan [1] for more details). That is, the shoreline horizontal position varies from $1-|\mathcal{A}|$ to $1+|\mathcal{A}|$.

3.5. More accurate approximations at the zero point of the spatial domain

In this subsection, we extend the Johns approximate solution, which is defined at $x=0$, to get more accurate approximations. We describe two ways to do this extension. The first is by formal expansion of stage w and velocity u with respect to the amplitude $\mathcal{A}$, and the second is by a fixed point iteration with a sea at rest ($w_0=0$, $u_0=0$) as the initial guess of the solution. (Please note that one may also use other standard methods, such as the Newton–Raphson method, for solving a system of equations to do an extension of the Johns approximate solution.)

The extension by formal expansion follows. Suppose that we are interested in getting an approximation that is quadratic with respect to the amplitude $\mathcal{A}$. The motivation is that we want to add an extra term to the approximate prescription (35) of Johns [5], so that it results in a new approximation that is a second order of accuracy. Let

$$w = w(\mathcal{A}) = W_0 + W_1\mathcal{A} + W_2\mathcal{A}^2 + O\left(\mathcal{A}^3\right), \tag{38}$$

$$u = u(\mathcal{A}) = U_0 + U_1\mathcal{A} + U_2\mathcal{A}^2 + O\left(\mathcal{A}^3\right) \tag{39}$$

be defined for some functions $W_0, W_1, W_2, \ldots$ and $U_0, U_1, U_2, \ldots$. Substituting Equations (38) and (39) into Equations (22) and (23) and neglecting the $O\left(\mathcal{A}^3\right)$ terms that are the cubic and higher order terms, we find the quadratic approximation of the stage w and the quadratic approximation of the velocity u given by

$$\begin{aligned} w = {} & \mathcal{A}J_0\left(\frac{4\pi}{T}\right)\cos\left(\frac{2\pi t}{T}\right) \\ & -\mathcal{A}^2\left[\frac{2\pi}{T}J_0\left(\frac{4\pi}{T}\right)J_1\left(\frac{4\pi}{T}\right)\cos\left(\frac{4\pi t}{T}\right)+\frac{1}{2}J_1^2\left(\frac{4\pi}{T}\right)\sin^2\left(\frac{2\pi t}{T}\right)\right], \end{aligned} \tag{40}$$

DOI: 10.1002/fld

$$u = -\mathcal{A}J_1\left(\frac{4\pi}{T}\right)\sin\left(\frac{2\pi t}{T}\right) + \mathcal{A}^2\left[\frac{\pi}{T}J_1^2\left(\frac{4\pi}{T}\right) - \frac{\pi}{T}J_0^2\left(\frac{4\pi}{T}\right) + \frac{1}{2}J_0\left(\frac{4\pi}{T}\right)J_1\left(\frac{4\pi}{T}\right)\right]\sin\left(\frac{4\pi t}{T}\right). \tag{41}$$

It should be stressed that the linearized w, given by Equation (35), of Johns [5] can be derived using the same process but neglecting the $O\left(\mathcal{A}^2\right)$ term that is the quadratic and higher order terms of the expansions (38) and (39).

The extension of the Johns approximate solution through a fixed point iteration follows. Based on Equations (22) and (23), we define kth level approximations of w and u at $x=0$

$$w_k = -\frac{1}{2}u_{k-1}^2 + \mathcal{A}J_0\left(\frac{4\pi\sqrt{w_{k-1}+1}}{T}\right)\cos\left(\frac{2\pi\left(u_{k-1}+t\right)}{T}\right), \tag{42}$$

and

$$u_k = -\frac{\mathcal{A}J_1\left(\frac{4\pi\sqrt{w_{k-1}+1}}{T}\right)}{\sqrt{w_{k-1}+1}}\sin\left(\frac{2\pi\left(u_{k-1}+t\right)}{T}\right), \tag{43}$$

for $k=1,2,...$, where $w_0=0$, $u_0=0$. These approximations are constructed recursively with a sea at rest ($w_0=0$, $u_0=0$) as the initial guess of the solution. As long as the Jacobian $\partial(x,t)/\partial(\sigma,\lambda)$ does not vanish in $\sigma>0$ (as mentioned in Subsection 3.1), we know that Equations (22) and (23) are single valued. Therefore, if the fixed point iteration converges, then it converges to the unique solution of the problem. Notice that here the first level recursive approximation w_1 of w is the approximate prescription (35) of Johns [5]. The second level recursive approximation w_2 of w and the second level recursive approximation u_2 of u are explicitly given by

$$w_2 = -\frac{1}{2}\left[\mathcal{A}J_1\left(\frac{4\pi}{T}\right)\sin\left(\frac{2\pi t}{T}\right)\right]^2 + \mathcal{A}J_0\left(\frac{4\pi\sqrt{\mathcal{A}J_0\left(\frac{4\pi}{T}\right)\cos\left(\frac{2\pi t}{T}\right)+1}}{T}\right)\cos\left(\frac{2\pi\left[t-\mathcal{A}J_1\left(\frac{4\pi}{T}\right)\sin\left(\frac{2\pi t}{T}\right)\right]}{T}\right), \tag{44}$$

$$u_2 = -\frac{\mathcal{A}J_1\left(\frac{4\pi\sqrt{\mathcal{A}J_0\left(\frac{4\pi}{T}\right)\cos\left(\frac{2\pi t}{T}\right)+1}}{T}\right)}{\sqrt{\mathcal{A}J_0\left(\frac{4\pi}{T}\right)\cos\left(\frac{2\pi t}{T}\right)+1}}\sin\left(\frac{2\pi\left(t-\mathcal{A}J_1\left(\frac{4\pi}{T}\right)\sin\left(\frac{2\pi t}{T}\right)\right)}{T}\right). \tag{45}$$

As mentioned by Johns [5], the exact solutions w and u can be computed by the use of Equations (22) and (23). However, it is impossible to *explicitly* write the exact solutions w and u. Therefore, if an explicit formulation of w is needed, such as for developing a numerical technique [5], we can take an approximation. We can take either the approximate solution (35) of Johns [5], our quadratic approximation (40), or our second level recursive approximation (44). Of course, we can have more accurate explicit approximations than the quadratic approximation (40) and the second level recursive approximation (44) by extending the approximate solution (35) of Johns [5] using either the formal expansion technique or fixed point iteration, but the formulations will be more complicated to write. Indeed, our approximate solutions (40) and (44) are more accurate than the approximate solution (35) of Johns [5].

4. COMPUTATIONAL EXPERIMENTS

In this section, we present the main results of computational experiments to achieve the goal of this paper. Based on these numerical experiments, we see that in some cases the Johns approximate solution (35) produces a large error.

DOI: 10.1002/fld

Johns [5] and Sidén and Lynch [6] applied the approximate prescription (35) to generate Carrier–Greenspan periodic waves. We claim the following: The Johns prescription (35) is not always a good approximation of the Carrier–Greenspan exact solution at $x^*=0$, and applying that approximate prescription at the fixed boundary to generate periodic waves using a numerical method may lead to a large error. A discrepancy between the Carrier–Greenspan exact solution and the Johns approximate solution (prescription) at $x^*=0$ must exist because of the linearization of Equation (22) to get Equation (37). To verify our claim, which is the goal of this paper, we investigate the discrepancy in two test cases: The first shows that the Johns prescription (35) is successful, and the second shows that the Johns prescription (35) fails to accurately approximate the Carrier–Greenspan exact solution at $x^*=0$. Note that, in this section, quantities are given in their dimensional values and measured in SI units.

Furthermore, for each test case, we compare three numerical solutions with respect to the exact solution in order to investigate the propagation of the prescription error. The first numerical solution is produced by a finite volume method (FVM) using the well-balanced scheme proposed by Audusse *et al.* [13] and extended by Noelle *et al.* [14] with the approximate prescription (35) of Johns [5] at $x^*=0$. The second numerical solution is produced by the same method using the same scheme but with the exact prescription (18) of Carrier and Greenspan at $x^*=0$. The third numerical solution is produced by the same method using the same scheme but with our proposed approximate prescription (44) at $x^*=0$.

In the finite volume method, here we use the best (among some other choices) numerical discretization given in our previous work [7]. That is, we choose a method based on the reconstruction of stage w^*, height h^*, and velocity u^*. We use the second order source, second order spatial (except at the prescribed cell where a first order discretization is taken), and second order temporal discretization. The minmod limiter is used for quantity reconstruction. We use the central upwind formulation developed by Kurganov, Noelle, and Petrova [8] to compute the numerical fluxes. The constant of gravitation is $g=9.81$. The minimum fluid height allowed in the flux computation is $h^*_{\min}=10^{-6}$. The uniform cell length is fixed and given by $\Delta x^*=100$ (except for testing the rate of convergence given in Section 5, in which we take various uniform cell lengths). The Courant–Friedrichs–Lewy number applied is 1.0. The discrete L^1 absolute error

$$E=\frac{1}{N}\sum_{i=1}^{N}|q(x_i)-Q_i| \tag{46}$$

is used to quantify the numerical error, where N is the number of cells, q is the exact quantity function, x_i is the centroid of the ith cell, and Q_i is the average value of quantity of the ith cell produced by the numerical method.

The prescribed cell is the first cell containing $x^*=0$ as its centroid. To be consistent with the work of Johns [5], at the first cell, if the linearized stage (35) of Johns is prescribed, we prescribe Equation (36) for the velocity; if the exact stage (18) of Carrier and Greenspan is prescribed, we take the exact velocity Equation (19) as the velocity prescription; and if the second level recursive approximation (44) of the stage is prescribed, the prescription (45) for the velocity is taken.

The numerical prescription is done as follows. Suppose that the linearized stage (35) of Johns [5] is prescribed (the prescription for Equations (18) and (44) are done similarly). Suppose that we are given time t^*. We compute the value $\bar{w}$ of the stage $w^*(t^*)$ and the value $\bar{u}$ of the velocity $u^*(t^*)$ at $x^*=0$ using the approximate prescriptions (35) and (36) of Johns [5]. Then we approximate the stage w^* and the velocity u^* for each spatial point x^* in the first cell using these values $\bar{w}$ and $\bar{u}$. This means that for this first cell, we take an approximation of the stage w^* and that of the velocity u^* that are constants with respect to spatial variable x^*. As a first order discretization of the bed topography is taken, we have constant (with respect to spatial variable x^*) approximations for all quantities (stage w^*, momentum p^*, velocity u, height h^*, and bed topography z^*) as our reconstruction for this first cell.

4.1. First test case: the Johns prescription is successful

In this subsection, we present a test case where the Johns prescription (35) successfully approximates the Carrier–Greenspan exact solution at $x^*=0$. We consider a spatial domain given by the

DOI: 10.1002/fld

interval $[-50, 55{,}050]$ discretized into 551 cells. The dimensional length $L^* = 50{,}000$, dimensional height $h_0^* = 500$, and dimensional period $T^* = 900$ are taken. Johns [5] took that at $x^* = 0$ the dimensional amplitude was $\epsilon^* = 1.0$, and we also take this value of ϵ^* in this test case. This setting implies that the shoreline position at any time lies on the interval [49,590.88, 50,409.12]. In a half of the period of oscillation, the shoreline travels a distance about 818.24.

When the Johns approximation (35), the quadratic approximation (40), and the second level recursive approximation (44) are prescribed at position $x^* = 0$ for time t^* on the interval $[0, T^*]$, discrepancies between each of those approximations and the Carrier–Greenspan exact solution occur. If we discretize the time interval $[0, T^*]$ into 1000 nodes, the average absolute discrepancy at $x^* = 0$ for stage w^* and velocity u^* are as given in Table I. Those discrepancies are very small, but obviously the quadratic approximation (40) and the second level recursive approximation (44) result in much smaller discrepancies. The results for the quadratic approximation (40) and the results for the second level recursive approximation (44) are about the same order.

Figure 2 illustrates the Carrier–Greenspan exact solution, the Johns approximate solution, and the second level recursive approximation for stage w^* and velocity u^* at position $x^* = 0$ for time t^* on the interval $[0, T^*]$. The discrepancies, in this case, are seen as negligible. We do not graphically show the results for the quadratic approximation because they are similar to the results for the second level recursive approximation.

Now, we investigate if the negligible discrepancy between the Carrier–Greenspan exact solution and the Johns approximate solution at $x^* = 0$ leads to a negligible discrepancy of any flow quantity

Table I. Average absolute discrepancies (errors) E at $x^* = 0$ when the setting of the first test case is taken. Here, the time interval $[0, T^*]$ is discretized into 1000 nodes. Subscripts w^* and u^* of E denote the average absolute discrepancy for stage w^* and velocity u^*, respectively.

Stage w prescription at $x^* = 0$	E_{w^*}	E_{u^*}
Johns approximation, Equation (35)	$1.35 \cdot 10^{-3}$	$1.20 \cdot 10^{-6}$
Quadratic approximation, Equation (40)	$2.29 \cdot 10^{-5}$	$1.78 \cdot 10^{-8}$
Second level recursive approximation, Equation (44)	$2.28 \cdot 10^{-5}$	$2.39 \cdot 10^{-8}$

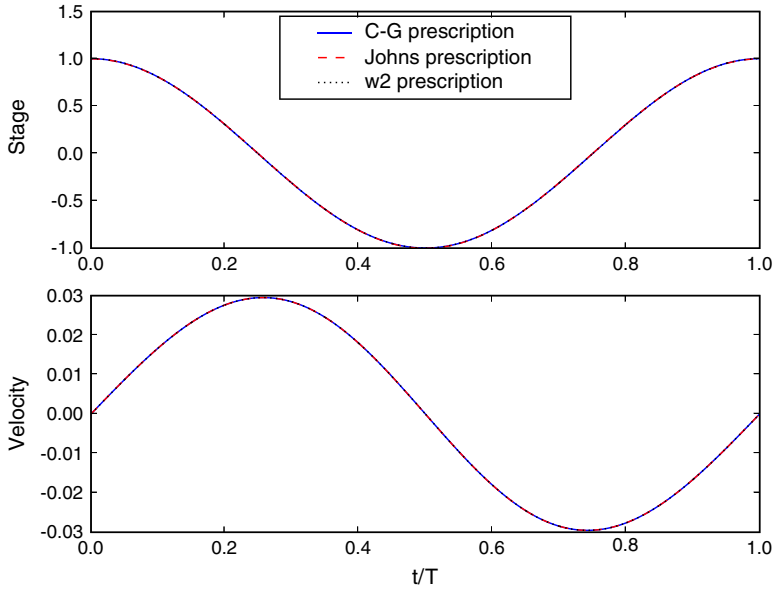

Figure 2. Prescriptions for w^* and u^* at $x^* = 0$. Here, $L^* = 50{,}000$, $h_0^* = 500$, $\epsilon^* = 1.0$, and $T^* = 900$. 'C–G prescription' stands for the Carrier–Greenspan exact prescription (18); 'Johns prescription' means the Johns prescription (35); 'w2 prescription' means the prescription of w_2 that is the second level recursive approximation (44).

DOI: 10.1002/fld

when those solutions at $x^*=0$ are prescribed in numerical simulations to generate periodic waves. We compare here the performance of the Johns approximate solution (35) and that of the second level recursive approximation (44). Starting from quiescent state, the numerical method generates a periodic solution after four periods of oscillation. The error comparison is presented in Table II. In general, the method with Carrier–Greenspan exact prescription results in smaller error. This is because the prescription discrepancy at $x^*=0$ propagates towards the shoreline as the time evolves, and consequently the error produced by the numerical method with the approximate prescription is larger than that produced by the numerical method with the exact prescription. However, we see that the discrepancies of the errors produced using the Johns prescription and Carrier–Greenspan exact prescription are small, as are the discrepancies of the errors produced using the second level recursive approximation and Carrier–Greenspan exact prescription. Figure 3 shows the stage w^*, momentum p^*, and velocity u^* at time $t^*=14T^*$. A large error in terms of the velocity occurs around the wet/dry interface: This is called the wet/dry interface or wetting and drying problem. It should be stressed that this problem is caused by the inaccuracy of the numerical method that we use at the wet/dry interface and does not relate to whether the prescription applied in the numerical simulation is exact or approximate. Through more recent research, we are working on this wet/dry interface problem to get a more accurate resolution. Some authors, such as Bollermann, Kurganov, and Noelle [9], Briganti and Dodd [10], Brufau, Vázquez-Cendón, and García-Navarro [11], and Gallardo, Parés, and Castro [12], have also attempted to resolve this wet/dry interface problem.

It is worth questioning why the discrepancy of the solutions at $x^*=0$ in this test case is negligible. This error is due to the small magnitude of the amplitude factor $\mathcal{A}$ in this test case. Recall that the amplitude factor $\mathcal{A}$ is found from the process of linearization of an equation discussed in Subsection 3.4. The linear approximation matches exactly with the exact solution when $\mathcal{A}=0$. In addition, a small magnitude of $\mathcal{A}$ leads to a small error of the linear approximation; a larger magnitude of $\mathcal{A}$ results in a larger error of the linear approximation.

Recalling the specified values of the dimensional length $L^*=50{,}000$, dimensional height $h_0^*=500$, and dimensional amplitude $\epsilon^*=1.0$, we can plot a graph relating the dimensional period T^* and the amplitude factor $\mathcal{A}$ as given in Figure 4 using Equation (37). The vertical lines in the figure are the asymptotes, which are the singularities of $\mathcal{A}$, that is, the zeros of the denominator in Equation (37). For $T^*=900$, the amplitude factor is $\mathcal{A}=-8.18\cdot 10^{-3}$.

Table II. Errors E for various times. Here, $L^*=50{,}000$, $h_0^*=500$, $\epsilon^*=1.0$, and $T^*=900$. Subscripts w^*, p^*, and u^* of E denote the error for stage w^*, momentum p^*, and velocity u^*, respectively. Superscript J of E denotes that the computation uses the Johns prescription, whereas superscript CG denotes that the computation uses Carrier–Greenspan exact prescription, and superscript w_2 denotes that the computation uses our w_2 approximate prescription.

Time (T^*)	$E^{\mathrm{J}}_{w^*}$	$E^{\mathrm{CG}}_{w^*}$	$E^{w_2}_{w^*}$	$E^{\mathrm{J}}_{p^*}$	$E^{\mathrm{CG}}_{p^*}$	$E^{w_2}_{p^*}$	$E^{\mathrm{J}}_{u^*}$	$E^{\mathrm{CG}}_{u^*}$	$E^{w_2}_{u^*}$
...	...	...	...	...	...	...	...	...	...
4	0.0130	0.0126	0.0127	0.686	0.679	0.679	0.0117	0.0114	0.0114
$4+1/3$	0.0138	0.0138	0.0138	0.693	0.693	0.694	0.0092	0.0090	0.0091
$4+2/3$	0.0161	0.0161	0.0161	0.500	0.480	0.481	0.0123	0.0122	0.0122
5	0.0119	0.0114	0.0114	0.643	0.636	0.636	0.0111	0.0109	0.0109
$5+1/3$	0.0117	0.0117	0.0117	0.648	0.648	0.649	0.0066	0.0065	0.0065
$5+2/3$	0.0119	0.0119	0.0119	0.393	0.376	0.376	0.0106	0.0106	0.0106
6	0.0076	0.0074	0.0074	0.413	0.409	0.409	0.0094	0.0092	0.0092
...	...	...	...	...	...	...	...	...	...
12	0.0072	0.0069	0.0070	0.244	0.246	0.246	0.0090	0.0088	0.0088
$12+1/3$	0.0053	0.0051	0.0051	0.360	0.364	0.365	0.0057	0.0056	0.0055
$12+2/3$	0.0084	0.0084	0.0084	0.220	0.226	0.226	0.0102	0.0103	0.0103
13	0.0072	0.0069	0.0070	0.245	0.246	0.246	0.0090	0.0088	0.0088
$13+1/3$	0.0053	0.0051	0.0051	0.360	0.364	0.365	0.0057	0.0056	0.0055
$13+2/3$	0.0084	0.0084	0.0084	0.220	0.225	0.226	0.0102	0.0103	0.0103
14	0.0072	0.0069	0.0070	0.245	0.246	0.246	0.0090	0.0088	0.0088
...	...	...	...	...	...	...	...	...	...

DOI: 10.1002/fld

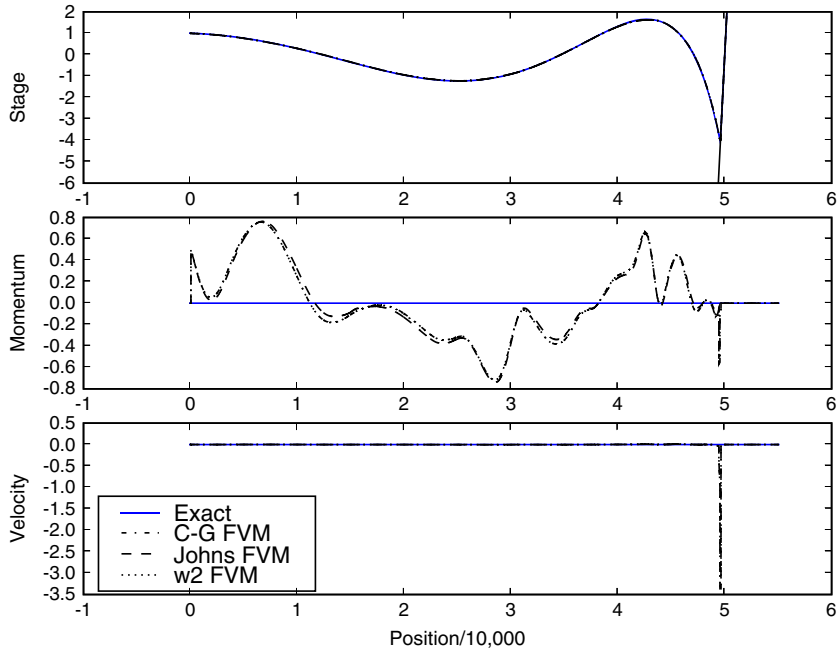

Figure 3. Solutions for w^*, p^*, and u^* at $t^* = 14T^*$. Here, $L^* = 50{,}000$, $h_0^* = 500$, $\epsilon^* = 1.0$, and $T^* = 900$. 'Exact' means the Carrier–Greenspan exact solution; 'C–G FVM' is the numerical solution by FVM with the exact prescription (18); 'Johns FVM' is the numerical solution by FVM with the Johns prescription (35); 'w2 FVM' is the numerical solution by FVM with the prescription of w_2 that is the second level recursive approximation (44).

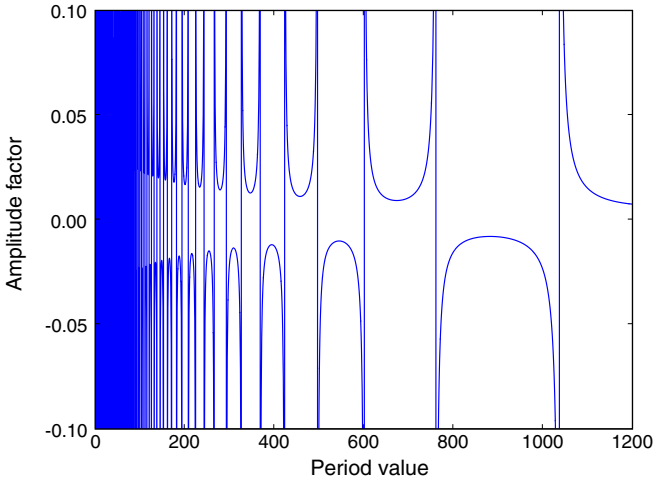

Figure 4. Relation of the dimensional period T^* and the amplitude factor $\mathcal{A}$ for $L^* = 50{,}000$, $h_0 = 500$, and $\epsilon^* = 1.0$. The vertical lines are asymptotes.

Roughly speaking, using the specified values of the dimensional length L^*, dimensional height h_0^*, and dimensional amplitude ϵ^* in this first test case, the Johns approximate solution (found by involving a linearization of an equation) at $x^* = 0$ is accurate on some intervals of the dimensional period T^*, such as $[800, 1000]$, where all points in this interval are far enough from asymptotes. This is illustrated in Figure 4 in which the tangent lines on the interval $[800, 1000]$, especially for points around $T^* = 900$, are almost horizontal.

Using the same values of the dimensional length L^*, dimensional height h_0^*, and dimensional amplitude ϵ^* but taking the dimensional period $T^* = 1020$, we find a larger discrepancy between the

DOI: 10.1002/fld

approximate and the exact solutions at $x^*=0$, as shown in Figure 5. Now, we have $\mathcal{A}=-5.26\cdot10^{-2}$. When we discretize the time interval $[0, T^*]$ into 1000 nodes, the average absolute discrepancy at $x^*=0$ for stage w^* and velocity u^* are $5.65\cdot10^{-2}$ and $1.30\cdot10^{-4}$, respectively, for the Johns approximate solution, and $3.16\cdot10^{-3}$ and $6.83\cdot10^{-6}$, respectively, for our second level approximation. These discrepancies for the Johns approximate solution are still relatively small. Unfortunately, if we take a larger value of T^* closer to the asymptote lying on the interval [1000, 1200] to get a larger value of $\mathcal{A}$, the Jacobian $\partial(x,t)/\partial(\sigma,\lambda)$ may vanish in $\sigma>0$, that is, a breaking wave occurs. The vanishing of the Jacobian $\partial(x,t)/\partial(\sigma,\lambda)$ can be verified analytically from Equations (11), (15), (16), and (17).

4.2. Second test case: the Johns prescription fails

In this subsection, we present a test case where the Johns prescription (35) fails to accurately approximate the Carrier–Greenspan exact solution at $x^*=0$. We consider a spatial domain given by the interval [−50, 65,050] discretized into 651 cells. The dimensional length $L^*=50{,}000$, dimensional height $h_0^*=500$, and dimensional period $T^*=3600$ are taken. We fix $\epsilon^*=5.0$ in this test case. We consider these values in order to get a larger value of amplitude factor $\mathcal{A}$ than the value of $\mathcal{A}$ in the first test case and that the Jacobian $\partial(x,t)/\partial(\sigma,\lambda)$ does not vanish in $\sigma>0$. Hence, the error of the Johns prescription (35) in this test case is larger than that in the first test case.

The setting here implies that the shoreline position at any time lies on the interval [38,745.65, 61,254.35] since $\mathcal{A}=-2.25\cdot10^{-1}$ and that no breaking wave occurs. In a half of the period of oscillation, the shoreline travels a distance more than $22.5\cdot10^3$. This distance is more than 27 times the distance traveled by the shoreline in the first test case. Recalling the specified values of the dimensional length L^*, dimensional height h_0^*, and dimensional amplitude ϵ^*, we plot the relation between the dimensional period T^* and the amplitude factor $\mathcal{A}$ in Figure 6.

When the Johns approximation (35), the quadratic approximation (40), and the second level recursive approximation (44) are prescribed at position $x^*=0$ for time t^* on the interval $[0, T^*]$, discrepancies between each of those approximations and the Carrier–Greenspan exact solution occur. Discretizing the time interval $[0, T^*]$ into 1000 nodes, we obtain that the average absolute discrepancy at $x^*=0$ for stage w^* and velocity u^* are as given in Table III. We see that the quadratic

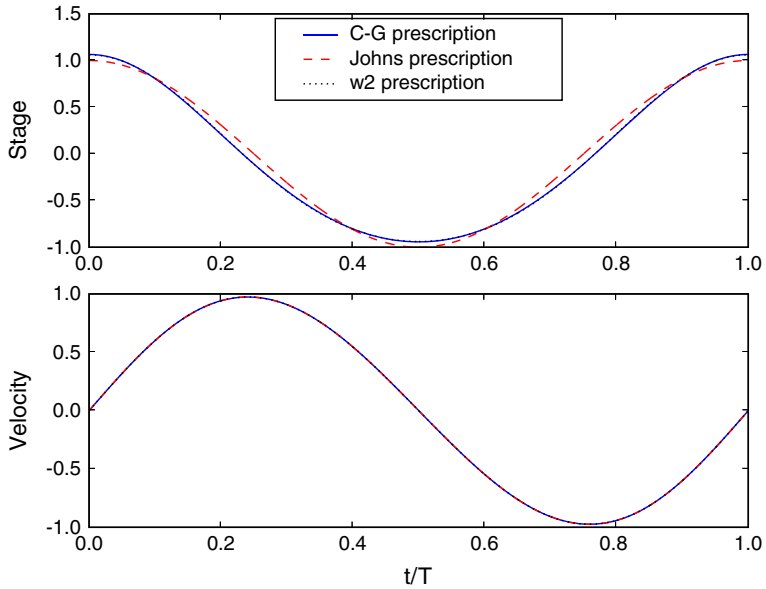

Figure 5. Solutions for w^* and u^* at $x^*=0$. Here, $L^*=50{,}000$, $h_0^*=500$, $\epsilon^*=1.0$, and $T^*=1020$. 'C–G prescription' stands for the Carrier–Greenspan exact prescription (18); 'Johns prescription' means the Johns prescription (35); 'w2 prescription' means the prescription of w_2 that is the second level recursive approximation (44).

DOI: 10.1002/fld

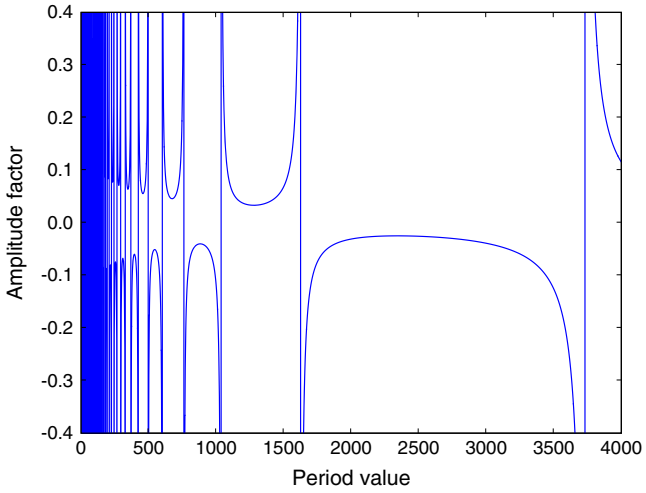

Figure 6. Relation of the dimensional period T^* and the amplitude factor $\mathcal{A}$ for $L^* = 50{,}000$, $h_0 = 500$, and $\epsilon^* = 5.0$. The vertical lines are asymptotes.

Table III. Average absolute discrepancies (errors) E at $x^* = 0$ when the setting of the second test case is taken. Here the time interval $[0, T^*]$ is discretized into 1000 nodes. Subscripts w^* and u^* of E denote the average absolute discrepancy for stage w^* and velocity u^*, respectively.

Stage w prescription at $x^* = 0$	E_{w^*}	E_{u^*}
Johns approximation, Equation (35)	1.83	$2.69 \cdot 10^{-2}$
Quadratic approximation, Equation (40)	$3.19 \cdot 10^{-1}$	$4.26 \cdot 10^{-3}$
Second level recursive approximation, Equation (44)	$2.88 \cdot 10^{-1}$	$3.85 \cdot 10^{-3}$

approximation (40) and the second level recursive approximation (44) results in much smaller discrepancies than the discrepancies that result from the Johns approximate solution (35). The results for the quadratic approximation (40) and the results for the second level recursive approximation (44) are again about the same order.

Figure 7 illustrates the Carrier–Greenspan exact solution, the Johns approximate solution, and the second level recursive approximation for stage w^* and velocity u^* at position $x^* = 0$ for time t^* on the interval $[0, T^*]$. The discrepancies that result from the Johns approximate solution are now large, whereas the discrepancies from the second level recursive approximation are much smaller. We do not graphically show the results for the quadratic approximation because they are similar to the results for the second level recursive approximation.

The method with the Johns prescription produces very large errors, as shown in Table IV. Large errors can also be observed graphically for the stage w^*, momentum p^*, and velocity u^* at time $t^* = 14T^*$, as illustrated in Figure 8. A magnification of Figure 8, depicting the stage w^* at cells around the wet/dry interfaces on the interval [38,400, 39,400], is shown in Figure 9. Notice that in Figure 9, the horizontal and the vertical distances from the wet/dry interface for the Carrier–Greenspan exact solution to the wet/dry interface for the numerical solution generated using the Johns prescription are about 500 and 5, respectively.

In this test case, the linearization of Equation (22) done by Johns [5] results in a poor approximation of the exact solution at $x^* = 0$. This poor approximation then leads to a very large error when it is prescribed in place of the Carrier–Greenspan exact solution at $x^* = 0$ to generate periodic waves in the numerical simulation. According to the simulation results, our second level recursive approximation (44) indeed produces smaller errors than the Johns approximate solution (35).

5. RATE OF CONVERGENCE

In this section, we present the rate of convergence of the numerical solution to the analytical solution using the exact boundary condition when the computational mesh is refined.

DOI: 10.1002/fld

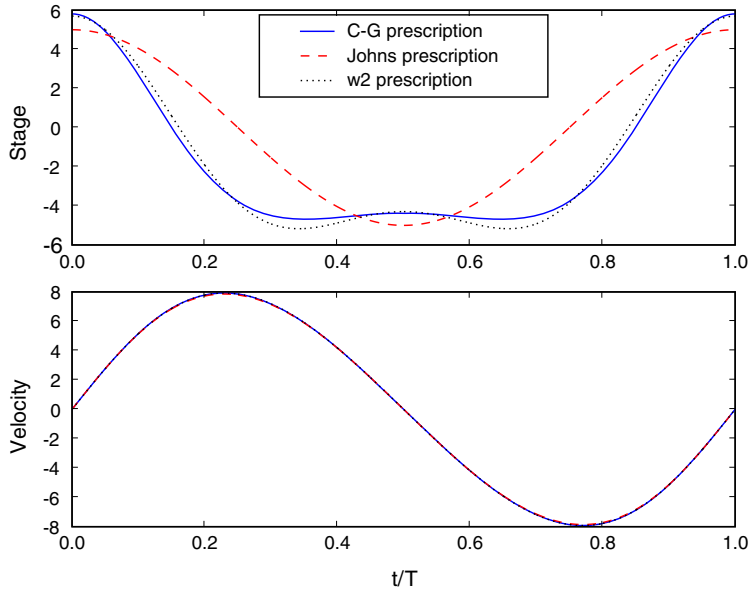

Figure 7. Solutions for w^* and u^* at $x^* = 0$. Here, $L^* = 50{,}000$, $h_0^* = 500$, $\epsilon^* = 5.0$, and $T^* = 3600$. 'C–G prescription' stands for the Carrier–Greenspan exact prescription (18); 'Johns prescription' means Johns prescription (35); 'w2 prescription' means the prescription of w_2 that is the second level recursive approximation (44).

Table IV. Errors E for various times. Here, $L^* = 50{,}000$, $h_0^* = 500$, $\epsilon^* = 5.0$, and $T^* = 3600$. Subscripts w^*, p^*, and u^* of E denote the error for stage w^*, momentum p^*, and velocity u^*, respectively. Superscript J of E denotes that the computation uses the Johns prescription, whereas superscript CG denotes that the computation uses Carrier–Greenspan exact prescription, and superscript w_2 denotes that the computation uses our w_2 approximate prescription.

Time (T^*)	$E^{\mathrm{J}}_{w^*}$	$E^{\mathrm{CG}}_{w^*}$	$E^{w_2}_{w^*}$	$E^{\mathrm{J}}_{p^*}$	$E^{\mathrm{CG}}_{p^*}$	$E^{w_2}_{p^*}$	$E^{\mathrm{J}}_{u^*}$	$E^{\mathrm{CG}}_{u^*}$	$E^{w_2}_{u^*}$
...	...	...	...	...	...	...	...	...	...
13	0.999	0.048	0.238	50.077	2.459	15.752	0.376	0.014	0.069
$13 + 1/6$	1.083	0.065	0.262	46.711	0.902	5.305	0.459	0.009	0.090
$13 + 2/6$	2.187	0.030	0.320	22.999	3.626	8.844	0.266	0.046	0.078
$13 + 3/6$	0.841	0.041	0.240	47.976	3.038	15.831	0.373	0.017	0.071
$13 + 4/6$	0.872	0.066	0.218	42.886	1.075	5.827	0.438	0.066	0.147
$13 + 5/6$	2.124	0.044	0.276	29.172	3.411	8.404	0.288	0.139	0.147
14	1.001	0.048	0.237	50.230	2.433	15.712	0.377	0.014	0.069
...	...	...	...	...	...	...	...	...	...

We expect that the numerical method leads to a first order of convergence because we take a first order discretization at the prescribed cell. Because of the wet/dry interface problem, the expected rate of convergence is not achieved, as can be observed in Table V. However, if we truncate the spatial domain in such a way that the computation does not involve the wet/dry interface problem, the numerical method we use indeed results in a first order of convergence, as shown in Table VI. This first order of convergence is observed because the errors produced by the numerical method are halved as the cell length is halved.

The results in Tables V and VI are found from simulations using the setting of the first test case given in Subsection 4.1. Recall that the shoreline position at any time lies on the interval [49,590.88, 50,409.12]. Therefore, the truncated domains in Table VI obviously do not include the moving boundary (shoreline). Consequently, all computations presented in Table VI do not involve the wet/dry interface problem. Note that a simulation with truncated domain here means that we prescribe the corresponding Carrier–Greenspan exact solution at cells located at both ends of the truncated domain; in addition, the domain is taken such that the centroid of the first cell is at $x^* = 0$.

DOI: 10.1002/fld

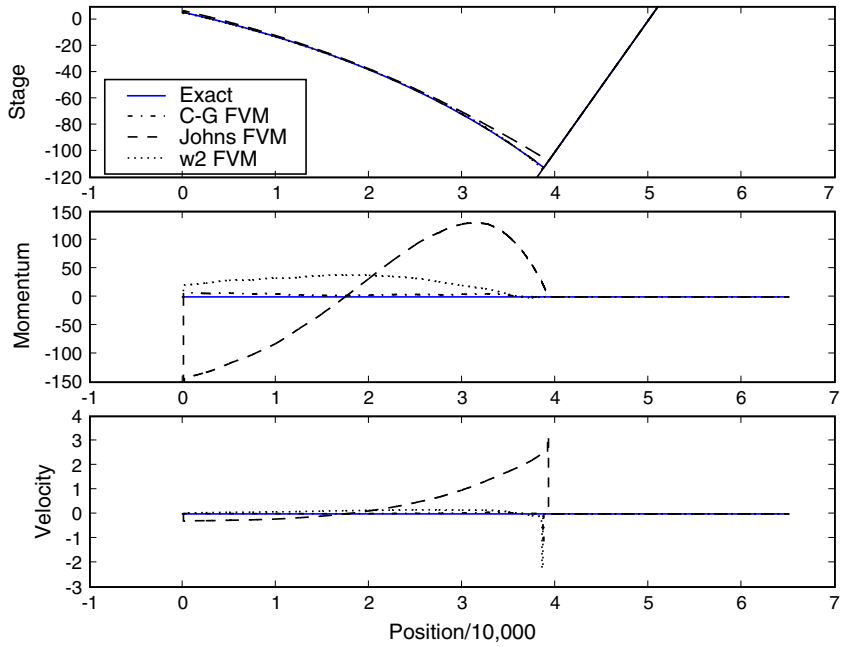

Figure 8. Solutions for w^*, p^*, and u^* at $t^* = 14T^*$. Here, $L^* = 50{,}000$, $h_0^* = 500$, $\epsilon^* = 5.0$, and $T^* = 3600$. 'Exact' means the Carrier–Greenspan exact solution; 'C–G FVM' is the numerical solution by FVM with the exact prescription (18); 'Johns FVM' is the numerical solution by FVM with the Johns prescription (35); 'w2 FVM' is the numerical solution by FVM with the prescription of w_2 that is the second level recursive approximation (44).

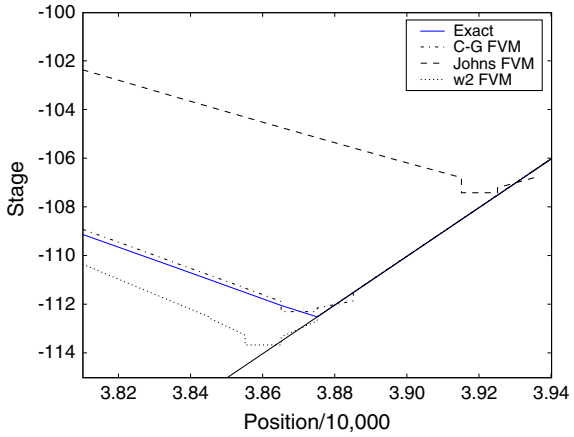

Figure 9. A magnification of Figure 8 for w^* on the interval [38,400, 39,400]. Here, $t^* = 14T^*$, $L^* = 50{,}000$, $h_0^* = 500$, $\epsilon^* = 5.0$, and $T^* = 3600$. 'Exact' means the Carrier–Greenspan exact solution; 'C–G FVM' is the numerical solution by FVM with the exact prescription; 'Johns FVM' is the numerical solution by FVM with the Johns prescription; 'w2 FVM' is the numerical solution by FVM with the prescription of w_2 that is the second level recursive approximation.

6. CONCLUSION

We have reviewed a special type of the Carrier–Greenspan solution, which can be used to test the performance of a numerical method for the shallow water wave equations. A new formula for the shoreline velocity has been derived. The new formula is very simple to use, as it involves no derivatives in calculating the shoreline velocity. We have also proposed some new approximations (a quadratic approximation and a second level recursive approximation) of the Carrier–Greenspan

DOI: 10.1002/fld

Table V. Errors E for various uniform cell lengths (Δx) of spatial discretization. Here, $L^* = 50{,}000$, $h_0^* = 500$, $\epsilon^* = 1.0$, and $T^* = 900$. Subscripts w^*, p^*, and u^* of E denote the error for stage w^*, momentum p^*, and velocity u^*, respectively. Superscript CG of E denotes that the computation uses Carrier–Greenspan exact prescription. Domain means the interval of spatial domain to be considered and discretized. The errors are computed at $t = 14T^*$.

Cell length	Domain	$E_{w^*}^{\mathrm{CG}}$ in 10^{-3}	$E_{p^*}^{\mathrm{CG}}$ in 10^{-2}	$E_{u^*}^{\mathrm{CG}}$ in 10^{-4}
200	[−100, 55,100]	23.84	88.19	254.05
100	[−50, 55,050]	6.95	24.64	88.12
50	[−25, 55,025]	2.13	13.19	35.25
25	[−12.5, 55,012.5]	1.36	9.36	8.42
12.5	[−6.25, 55,006.25]	1.26	7.24	6.23

Table VI. Errors E for various uniform cell lengths (Δx) of spatial discretization. Here, $L^* = 50{,}000$, $h_0^* = 500$, $\epsilon^* = 1.0$, and $T^* = 900$. Subscripts w^*, p^*, and u^* of E denote the error for stage w^*, momentum p^*, and velocity u^*, respectively. Superscript CG of E denotes that the computation uses Carrier–Greenspan exact prescription. Domain means the interval of spatial domain to be considered and discretized. The errors are computed at $t = T^*$.

Cell length	Domain	$E_{w^*}^{\mathrm{CG}}$ in 10^{-5}	$E_{p^*}^{\mathrm{CG}}$ in 10^{-2}	$E_{u^*}^{\mathrm{CG}}$ in 10^{-5}
200	[−100, 10,100]	97.17	48.94	110.98
100	[−50, 10,050]	46.42	25.13	56.99
50	[−25, 10,025]	22.68	12.73	28.87
25	[−12.5, 10,012.5]	11.55	6.39	14.49
12.5	[−6.25, 10,006.25]	5.80	3.20	7.26

periodic solution, which are more accurate than the Johns approximate solution at the zero point of the spatial domain. In addition, results of a finite volume method with the approximate prescriptions applied at the fixed boundary to generate periodic waves on a sloping beach have been compared with those of the same method with the Carrier–Greenspan exact prescription.

We have found that if the discrepancy between the approximate and the exact prescriptions is negligible, the errors of both numerical solutions are similar. If the discrepancy is very large, the error of the numerical solution with the approximate prescription is much larger than that of the numerical solution with the exact prescription. This means that the prescription at the fixed boundary significantly affects the error of the numerical solution. Therefore, we suggest that the exact, instead of the approximate prescription, should be applied when the Carrier–Greenspan periodic waves are used to assess the performance of a numerical method.

However, if an explicit formulation of the stage at the zero point of the spatial domain is needed, such as for developing a numerical technique, an approximation of it can be taken. We can take either the approximate solution of Johns, the quadratic approximation, the second level recursive approximation, or another approximation as long as it is guaranteed that the error produced at the zero point of the spatial domain is negligible.

ACKNOWLEDGEMENTS

We thank the reviewers for their insightful and constructive comments, which have significantly improved the quality of the manuscript. For helpful discussions that improved this writing technically, we thank Nick Gouth at the Mathematical Sciences Institute, The Australian National University (ANU). Some discussions with Christopher Zoppou at the ANU are also acknowledged. The work of Sudi Mungkasi was supported by ANU PhD and ANU Tuition Scholarships.

REFERENCES

1. Carrier GF, Greenspan HP. Water waves of finite amplitude on a sloping beach. *Journal of Fluid Mechanics* 1958; **4**(1):97–109.
2. Bellotti G, Brocchini M. On the shoreline boundary conditions for Boussinesq-type models. *International Journal for Numerical Methods in Fluids* 2001; **37**(4):479–500.

DOI: 10.1002/fld

3. Brocchini M, Svendsen IA, Prasad RS, Bellotti G. A comparison of two different types of shoreline boundary conditions. *Computer Methods in Applied Mechanics and Engineering* 2002; **191**(39–40):4475–4496.
4. Dietrich JC, Kolar RL, Luettich RA. Assessment of ADCIRC's wetting and drying algorithm. In *Proceedings of the 15th International Conference on Computational Methods in Water Resources (CMWR XV), Chapel Hill, 13–17 June 2004*, Vol. 2, Miller CT, Farthing MW, Gray WG, Pinder GF (eds). Elsevier: Amsterdam, 2004; 1767–1778.
5. Johns B. Numerical integration of the shallow water equations over a sloping shelf. *International Journal for Numerical Methods in Fluids* 1982; **2**(3):253–261.
6. Sidén GLD, Lynch DR. Wave equation hydrodynamics on deforming elements. *International Journal for Numerical Methods in Fluids* 1988; **8**(9):1071–1093.
7. Mungkasi S, Roberts SG. On the best quantity reconstructions for a well balanced finite volume method used to solve the shallow water wave equations with a wet/dry interface. *The Australian and New Zealand Industrial and Applied Mathematics Journal* 2010; **51**(EMAC2009):C48–C65.
8. Kurganov A, Noelle S, Petrova G. Semidiscrete central-upwind schemes for hyperbolic conservation laws and Hamilton–Jacobi equations. *SIAM Journal on Scientific Computing* 2001; **23**(3):707–740.
9. Bollermann A, Kurganov A, Noelle N. A well-balanced reconstruction for wetting/drying fronts. *IGPM Report* 2010; **313**:1–18.
10. Briganti R, Dodd N. Shoreline motion in nonlinear shallow water coastal models. *Coastal Engineering* 2009; **56**(5–6):495–505.
11. Brufau P, Vázquez-Cendón ME, García-Navarro P. A numerical model for the flooding and drying of irregular domains. *International Journal for Numerical Methods in Fluids* 2002; **39**(3):247–275.
12. Gallardo JM, Parés C, Castro M. On a well-balanced high-order finite volume scheme for shallow water equations with topography and dry areas. *Journal of Computational Physics* 2007; **227**(1):574–601.
13. Audusse E, Bouchut F, Bristeau MO, Klein R, Perthame B. A fast and stable well-balanced scheme with hydrostatic reconstruction for shallow water flows. *SIAM Journal on Scientific Computing* 2004; **25**(6):2050–2065.
14. Noelle S, Pankratz N, Puppo G, Natvig JR. Well-balanced finite volume schemes of arbitrary order of accuracy for shallow water flows. *Journal of Computational Physics* 2006; **213**(2):474–499.

DOI: 10.1002/fld